Breakup-fusion analyses of the ^{40}Ca(^{6}Li,d)^{44}Ti reactions and α-cluster structure in ^{44}Ti

Chong-Yeal Kim and T. Udagawa
Department of Physics, University of Texas, Austin, Texas 78712
(Received 6 April 1992)

Analyses of data of the ^{40}Ca(^{6}Li,d)^{44}Ti reactions at incident energies of 28 and 50 MeV have been carried out within the framework of the breakup-fusion approach, which allows us to treat reactions to both bound and unbound final states on a single footing. The resultant spectroscopic information, particularly concerning the α-cluster structure of ^{44}Ti, is presented and discussed.

PACS number(s): 21.60.Gx, 24.50.+g, 25.70.Hi, 27.40.+z

I. INTRODUCTION

In a recent study [1,2], we have made use of the breakup-fusion (BF) description in the calculation of spectra of the single nucleon stripping type [^{27}Al(d,p), ^{62}Ni(d,p), and ^{144}Sm(α,t)] reactions leading to both bound ($E_x<0$, where E_x is the energy of the stripped particle) and unbound ($E_x>0$) regions. The method allows us to analyze the data of both regions on a single footing, without introducing a bound state approximation for dealing with the unbound states. It was shown that the calculated spectra fit the data in both regions very nicely. The method was also capable of providing spectroscopic information on high-lying single particle states. In fact, in Ref. [2] we were able to identify the $f_{7/2}$ state in ^{28}Al, the $d_{3/2}$ state in ^{63}Ni, and the $f_{7/2}$, $h_{9/2}$, and $i_{13/2}$ states in ^{145}Eu. Note that the single particle states identified in ^{145}Eu are all in the continuum region.

In the present paper, we apply the same BF method to analyze data for the α-transfer ^{40}Ca(^{6}Li,d)^{44}Ti reactions at incident energies of $E_{\rm lab}=28$ and 50 MeV [3,4]. The aim is to extract spectroscopic information, particularly on the α-cluster structure of ^{44}Ti that has been a current issue in α-cluster structure studies [5–10]. Since many of the α-cluster states appear in the unbound region, the BF method may be the most suitable to be used for that purpose.

We note that the data to be analyzed in the present study have all been analyzed [3,4] before with the distorted wave Born approximation (DWBA). The analyses were, however, made separately, using different sets of the optical potentials. In particular, the 50 MeV data were analyzed [4] with optical potentials that are dramatically different from the elastic potentials. Because of this, as we shall confirm in this study, the spectroscopic factors obtained in Ref. [4] are smaller by an order of magnitude than those obtained in Ref. [3]. In the present study, we try to analyze the data at both energies on the same footing, using the elastic potentials whenever possible.

Another important aspect of the present work is in a recent advance in the "unique optical potential" for the α-^{40}Ca system. Delbar *et al.* [11] achieved an unambiguous determination of the real part of the potential from an extensive analysis of elastic scattering data extending from $E_\alpha=24$ to 166 MeV. Later, this "unique potential" was shown to describe not only the scattering data, but also α-cluster states in the bound and low energy unbound regions [5]. In the present study, use is made of this "unique potential" that provides a unified description of the α-^{40}Ca system in both bound and unbound regions. Our hope is that in this way we may deduce quantitative information on the α-cluster structure of ^{44}Ti.

In Sec. II, we summarize the BF formulas that are relevant to the present calculation. There, also, a discussion is given on the relation between the present calculation and the usual DWBA stripping calculation. The results of the analysis of the experimental data are presented in Sec. III. Based on the results, we discuss in Sec. IV the α-cluster structure of the final nucleus ^{44}Ti. Finally, Sec. V will be devoted to a summary of our work.

II. FORMULATION OF BREAK-FUSION CALCULATIONS

The breakup-fusion (BF) reaction that we consider in the present study may be written symbolically as

$$^{6}\mathrm{Li}+^{40}\mathrm{Ca}\rightarrow d+\alpha+^{40}\mathrm{Ca}\rightarrow d+^{44}\mathrm{Ti}\ . \tag{1}$$

In Eq. (1), the first step (indicated by the first arrow) denotes the breakup of ^{6}Li into $d+\alpha$, while the second step stands for the subsequent fusion (or capture) of α into the target ^{40}Ca to form the residual nucleus ^{44}Ti. We assume that the particles (d, α, and ^{40}Ca) involved in the first breakup step are all in their ground states. This means that the first step is assumed to be what is called an elastic breakup (EB). In the following, we intend to give the formula for the singles cross section for d in the reaction Eq. (1).

Let us denote the excitation energy of the residual nucleus ^{44}Ti by $E_{\rm ex}$. If the energy carried by the particle i ($i=^{6}$Li, d, and α) is denoted by E_i, $E_{\rm ex}$ is expressed as

$$E_{\rm ex}=E_\alpha+Q_3-Q_g=E_{\rm Li}-E_d-Q_g\ . \tag{2}$$

Here Q_g and Q_3 are the Q values, respectively, of the stripping reaction ^{40}Ca(^{6}Li,d)^{44}Ti and of the three-body breakup.

We shall call the systems consisting of ^{6}Li+^{40}Ca, $d+^{44}$Ti, and $\alpha+^{40}$Ca the ^{6}Li, d, and α-channels, respectively. The distorted waves $\chi_i^{(+)}$ [and $\chi_i^{(-)*}(\mathbf{k},\mathbf{r})$

$=\chi_i^+(-\mathbf{k},\mathbf{r})$] in these channels are given as solutions of the optical model Schrödinger equation

$$(E_i-T_i-U_i)\chi_i^{(+)}=0 \ . \tag{3}$$

Here T_i and U_i are, respectively, the kinetic energy operator and the optical model potential.

The double differential BF cross section is given as

$$\frac{d^2\sigma^{\rm BF}}{dE_d d\Omega_d}=\sum_{l_\alpha}\frac{d^2\sigma^{\rm BF}_{l_\alpha}}{dE_d d\Omega_d} \ , \tag{4}$$

where

$$\frac{d^2\sigma^{\rm BF}_{l_\alpha}}{dE_d d\Omega_d} =\frac{2\pi}{\hbar v}|C^{(2)}|^2\rho(E_d)\sum_{m_{l_\alpha}}[\langle u_{l_\alpha m_{l_\alpha}}|-W_\alpha|u_{l_\alpha m_{l_\alpha}}\rangle/\pi] \tag{5}$$

is the partial wave cross section. In Eqs. (4) and (5), l_α and m_{l_α} are, respectively, the orbital angular momenta of α and its z component. l_α serves as a transfer angular momentum of the reaction. $C^{(2)}$ in (5) is the spectroscopic amplitude for the ^{6}Li$\rightarrow d+\alpha$ process, while $\rho(E_d)$ is the phase space volume of the emitted particle d, and is given by

$$\rho(E_d)=\frac{\hbar^2 k_d}{(2\pi)^3\mu_d} \ . \tag{6}$$

k_d and μ_d in the above equation are the wave number and the reduced mass of d, respectively.

Further in (5), v is the relative velocity in the incident channel, while W_α is the imaginary part of U_α $(=V_\alpha+iW_\alpha)$. The function $u_{l_\alpha m_{l_\alpha}}(r)$ is the α-channel partial wave function that describes the motion of α with respect to ^{40}Ca. It satisfies the inhomogeneous equation

$$(h_\alpha-E_\alpha)u_{l_\alpha m_{l_\alpha}}(r)=\rho_{l_\alpha m_{l_\alpha}}(r) \ , \tag{7}$$

with

$$h_\alpha=-\frac{\hbar^2}{2\mu_\alpha}\left[\frac{d^2}{dr^2}-\frac{l_\alpha(l_\alpha+1)}{r^2}\right]+U_\alpha \ . \tag{8}$$

$\rho_{l_\alpha m_{l_\alpha}}(r)$ on the right-hand side of Eq. (7) is the source function (for creating the particle α) and is defined as

$$\rho_{l_\alpha m_{l_\alpha}}(r)=r\langle\chi_d^{(-)}i^{l_\alpha}Y_{l_\alpha m_{l_\alpha}}|\mathcal{V}|\chi^{(+)}_{^6{\rm Li}}\phi_{d\alpha}\rangle \ . \tag{9}$$

Here $Y_{l_\alpha m_{l_\alpha}}$ is a spherical harmonic, while $\phi_{d\alpha}$ is the wave function for the relative motion between d and α in ^{6}Li. The symbol ($\|$) in (9) is used to denote that the integration is taken over all coordinates except the α-channel coordinate $\mathbf{r}_\alpha$. Furthermore, $\mathcal{V}$ is the residual interaction given by

$$\mathcal{V}=U_\alpha+U_d-U_{\rm Li} \ . \tag{10}$$

The formulas given above can be used for both $E_\alpha>0$ and $E_\alpha<0$ cases. The only care that has to be taken is that in solving Eq. (7) an outgoing boundary condition is to be imposed upon $u_{l_\alpha m_{l_\alpha}}$ for $E_\alpha>0$, while an exponentially decaying boundary condition is to be imposed for $E_\alpha<0$.

For the $E_\alpha<0$ case, the BF cross section given by Eq. (4) is by itself the deuteron singles cross section. For the $E_\alpha>0$ case, however, the cross section for the EB reaction must be added to the BF cross section. This EB cross section can be given, using notation already explained, as

$$\frac{d^2\sigma^{\rm EB}}{dE_d d\Omega_d}=\sum_{l_\alpha}\frac{d^2\sigma^{\rm EB}_{l_\alpha}}{dE_d d\Omega_d} \ , \tag{11}$$

$$\frac{d^2\sigma^{\rm EB}_{l_\alpha}}{dE_d d\Omega_d}=\frac{2\pi}{\hbar v}\rho(E_d)|C^{(2)}|^2 \times\sum_{m_{l_\alpha}}\left|\frac{4\pi}{\hbar k_d}\int\chi^{(-)*}_{l_\alpha}(r)\rho_{l_\alpha m_{l_\alpha}}(r)dr\right|^2 \ . \tag{12}$$

The total singles cross section can then be given as a sum of the BF and EB cross sections, i.e.,

$$\frac{d^2\sigma}{dE_d d\Omega_d}=\frac{d^2\sigma^{\rm BF}}{dE_d d\Omega_d}+\frac{d^2\sigma^{\rm EB}}{dE_d d\Omega_d} \ . \tag{13}$$

A similar relation holds for each of the partial wave cross sections,

$$\frac{d^2\sigma_{l_\alpha}}{dE_d d\Omega_d}=\frac{d^2\sigma^{\rm BF}_{l_\alpha}}{dE_d d\Omega_d}+\frac{d^2\sigma^{\rm EB}_{l_\alpha}}{dE_d d\Omega_d} \ . \tag{14}$$

Although the numerical calculations performed in the next section are carried out by using the formulas given above, it is instructive to present here more simplified formulas which can be obtained by assuming that W_x takes a constant value $\Gamma/2$. As shown in Ref. [2], the partial BF cross section can then be rewritten as

$$\frac{d^2\sigma_{l_\alpha}}{dE_d d\Omega_d}=\sum_{n_\alpha l_\alpha}S_{n_\alpha l_\alpha}(E)\left[\frac{d\sigma_{n_\alpha l_\alpha}}{d\Omega_d}\right]^{\rm DW} \ , \tag{15}$$

where $(d\sigma_{n_\alpha l_\alpha}/d\Omega_d)^{\rm DW}$ is the familiar (DWBA) cross section for the stripping reaction [12] in which the transferred particle α is captured into the single particle orbital specified by a set of quantum number $(n_\alpha l_\alpha)$, n_α being the radial node. $(d\sigma_{n_\alpha l_\alpha}/d\Omega_d)^{\rm DW}$ can be explicitly written as

$$\left[\frac{d\sigma_{n_\alpha l_\alpha}}{d\Omega_d}\right]^{\rm DW}=\frac{2\pi}{\hbar v}\rho(E_d) \times\sum_{m_\alpha}|\langle\chi_d^{(-)}\psi_{n_\alpha l_\alpha m_\alpha}|\mathcal{V}|\chi^{(+)}_{^6{\rm Li}}\phi_{d\alpha}\rangle|^2 \ . \tag{16}$$

Further $S_{n_\alpha l_\alpha}(E)$ in Eq. (15) is the spectroscopic strength function defined as

$$S_{n_\alpha l_\alpha}(E)=\frac{\Gamma}{2\pi}\frac{1}{(E-E_{n_\alpha l_\alpha})^2+\Gamma^2/4} . \quad (17)$$

$\psi_{n_\alpha l_\alpha m_\alpha}$ in Eq. (16) and $E_{n_\alpha l_\alpha}$ in Eq. (17) are the wave function and energy of the single α-cluster state labeled by $(n_\alpha l_\alpha)$ and satisfy the following Schrödinger equation with h_α defined by Eq. (8):

$$(h_\alpha-E_{n_\alpha l_\alpha})\psi_{n_\alpha l_\alpha m_\alpha}=0 . \quad (18)$$

The sum over $(n_\alpha l_\alpha)$ involved in Eq. (15) is taken over the complete set of solutions of the above equation, including the continuum states. It is thus clear that the resultant cross section given by Eq. (15) with Eqs. (16) and (17) is nothing but an energy averaged DWBA cross section. The energy average results from our inclusion of the imaginary (spreading) part W_α in the α potential. The two-step description involved in the BF approach allows us to take this into account automatically. In the limit of $\Gamma\to 0$, $S_{n_\alpha l_\alpha}(E)$ becomes a δ function and hence the cross section Eq. (15) is reduced to that of discrete peaks.

III. NUMERICAL CALCULATIONS AND ANALYSES OF EXPERIMENTAL DATA

A. Choice of theoretical parameters

There are not many theoretical parameters involved in the present calculation; the most important are those of the optical potentials in the ^{6}Li, d, and α channels. These parameters are fairly well known, except those of the α-spreading potential W_α in the bound ($E_\alpha<0$), and the unbound but small E_α region. We can therefore take most of the parameters from published literature; those for the ^{6}Li and d potentials are taken from Chua *et al.* [13] and Daenick *et al.* [14], respectively. These parameters were determined from the analyses of elastic scattering data (elastic potential). In the case of the deuteron, such an elastic potential has been determined for the whole energy region considered in the present study. For the case of ^{6}Li, however, the elastic potential is available only for $E_{\rm lab}=50$ MeV. We use here the 50 MeV potential also for the 28 MeV case.

As already mentioned in the Introduction, use is made of the "unique optical potential" by Delbar *et al.* [11] for the α potential. The potential can reproduce not only the α-^{40}Ca scattering data, but also the experimental energies of the low-lying bound α-cluster states in the ^{44}Ti system [5]. Note, however, the imaginary (spreading) part W_α of the potential is not well known for the energy region ($E_\alpha=-5.2-10$ MeV) considered in the present study. Fortunately, the result of the analysis does not depend very much on the choice of W_α. Therefore we simply assume here a weak potential for W_α. In Table I we summarize the values of the parameters used in the present calculations.

Another parameter involved is the potential $V_{d\alpha}$ for generating the bound state wave function $\phi_{d\alpha}$. For this, we use the same Woods-Saxon potential as used in Ref. [4] with the diffuseness and radius parameters of $a=0.65$ fm and $r_0=1.20$ fm, respectively. The strength is then fixed so as to reproduce the experimental separation energy (1.47 MeV) of ^{6}Li, assuming that the radial wave function of ^{6}Li has the node $n=1$. The $V_{d\alpha}$ value thus fixed is $V_{d\alpha}=104$ MeV.

The last parameter is the spectroscopic factor $|C^{(2)}|^2$ for the breakup of ^{6}Li into $\alpha+d$. The factor is quite important for the determination of the absolute magnitude of the α spectroscopic factor S_i [see Eq. (20) for the definition] that we wish to extract from the experimental data. There are many experimental and theoretical studies [15,16] made of this factor. Quoting the most recent experimental value [15], it is $|C^{(2)}|^2=0.73$. On the other hand, the theoretical values are 0.85–1.0 [16]. There is an obvious difference between the experimental and theoretical values, but both are fairly close to unity. In the present study, we tentatively set $|C^{(2)}|^2=1$. This may lead to an underestimation of the α-particle spectroscopic factors, but it is easy to make appropriate corrections, if and when a more precise $|C^{(2)}|^2$ value becomes available.

B. Lower cutoff procedure

With the elastic potentials discussed in Sec. III A, however, it has been difficult to reproduce observed angular distributions, particularly those at 50 MeV. For this reason, Yamaya *et al.* [4] introduced a quite large modification into the radius parameters of the real part of the potentials; the radius parameters of both ^{6}Li and d potentials were changed from their elastic values of 1.30 and 1.05 to 1.05 and 1.35 fm, respectively. As will be discussed later in the next section, this modification results in unreasonably small α spectroscopic factors.

It has been found, however, that the observed angular distributions can be reproduced with the elastic poten-

TABLE I. Optical potential parameters. The potentials for the ^{6}Li and d channels are those of the usual Woods-Saxon potential, while that for the α channel is the squared Woods-Saxon potential. The energy dependence is taken into account for the d-channel potential. Note that E is the deuteron laboratory energy in MeV and $\beta=-(E/100)^2$.

	V_0 (MeV)	r_0 (fm)	a_0 (fm)	W_V (MeV)	W_S (MeV)	r_I (fm)	a_I (fm)	r_C (fm)	Ref.
^{6}Li	244.0	1.30	0.7	23.5	0.0	1.7	0.9	1.4	[13]
d	$94-0.26E$	1.17	$0.709+0.0017E$	$(12.2+0.026E)\times(1-e^\beta)$	$(12.2+0.026E)\times e^\beta$	1.325	0.762	1.3	[14]
α	182.4	1.37	1.29	0.0	0.5	1.75	1.0	1.3	[11]

tials, if a "lower cutoff" is introduced in the integration over radial coordinate r_α of the α channel. At this moment the origin of this cutoff has not been fully understood, but it may arise from the nonlocality of the α-particle optical potential [9]. As is well known, the nonlocality effectively reduces contribution to the cross section from the nuclear interior [17]. Another origin may lie in the possibility that the simple cluster description in terms of the α single particle potential is valid only in the nuclear exterior. In fact, it has been suggested that alpha clustering may be favored in the nuclear surface [18]. In the present study, we shall not go further into this problem, except that we shall show later (see Fig. 4) some example calculations that indicate the sensitivity of the calculated cross sections to the radial cutoff parameter R_c. We utilize this cutoff procedure for fitting the calculated cross section to experiment.

C. Double differential cross sections and unit single particle cross sections

Figure 1 shows the calculated double differential cross sections at $\theta=0°$ for all l_α values considered in this study, taking, as an example, the $E_\alpha=50$ MeV case. The lower cutoff parameters R_c used in the calculation are given in the figure. Because of the use of the weak W_α (see Table I), the resultant spectra become very sharply peaked. In the cross sections for $l_\alpha \leq 4$, we observe two peaks in the energy domain considered, one in the bound and the other in the unbound region, separated by about 10 MeV. The lower states are those of the oscillator total quantum number $N=12$ where $N=2n_\alpha+l_\alpha$, while the higher states are those of $N=14$. The lowest peak appearing in the $l_\alpha=0$ spectrum at $E_x=-4.5$ MeV corresponds to that of the ground state. All the peak positions including that of the ground state agree with those predicted earlier in Refs. [5] and [7]. Note that the contribution from the EB process is negligible in the energy range considered in Fig. 1.

The double differential cross sections as shown in Fig. 1 are generated for other angles. Single differential cross sections for each peak specified by a set of the quantum numbers (n_α,l_α) are then obtained by integrating the double differential cross section over the peak as

$$\frac{d\sigma_{n_\alpha l_\alpha}}{d\Omega_d}=\int_{E_{n_\alpha l_\alpha}-\Delta}^{E_{n_\alpha l_\alpha}+\Delta}\frac{d^2\sigma_{l_\alpha}}{dE_\alpha d\Omega_d}\,, \tag{19}$$

where Δ measures the interval of the integration that covers the resonance. We shall use $d\sigma_{n_\alpha l_\alpha}/d\Omega_d$ defined

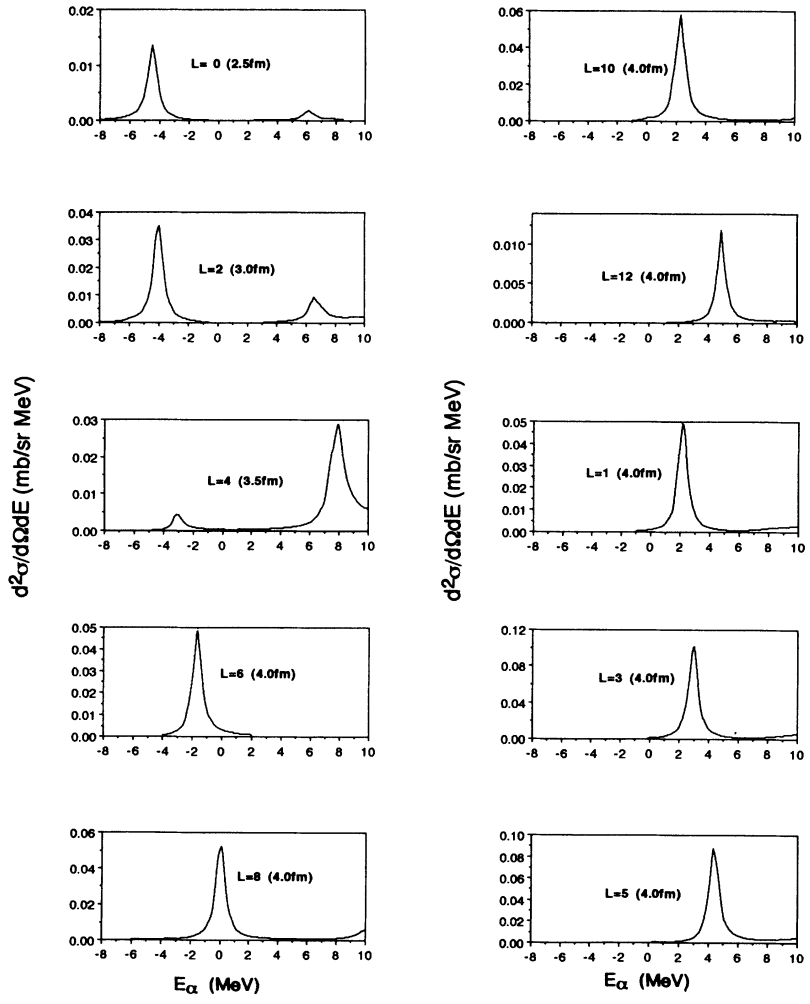

FIG. 1. Calculated double differential cross sections at $\theta=0°$ as a function of E_α. The two peaks seen correspond to those of $N=12$ and 14 cluster states.

above as our unit single particle cross sections for analyzing the data. Note that $d\sigma_{n_\alpha l_\alpha}/d\Omega_d$ is similar to the usual single particle DWBA cross section. The merit of the use of the BF method for obtaining $d\sigma_{n_\alpha l_\alpha}/d\Omega_d$ lies in the fact that one can generate cross sections in the bound and unbound region on the same footing, without introducing, for instance, a bound state approximation in the unbound region.

D. Results of analyses

We now analyze the data of the ^{40}Ca(^{6}Li,d)^{44}Ti reaction at $E_{\rm lab}=28$ and 50 MeV [3,4]. The data are available for excitation energies up to about $E_{\rm ex}=8$ and 11 MeV, for $E_{\rm lab}=28$ and 50 MeV cases, respectively. Note that the α emission threshold energy ($E_\alpha=0.0$ MeV) corresponds to $E_{\rm ex}=5.12$ MeV. This means that we deal here with the data for $E_\alpha=-5.1$ to 5.9 MeV for the case of the $E_{\rm lab}=50$ MeV.

In the region of $E_{\rm ex}=0.0-11$ MeV, the energy spectrum of ^{44}Ti is discrete; all the observed levels are isolated. This is due to the fact that even the highest excitation energy (11 MeV) considered is still much lower than the Coulomb-barrier height (16 MeV) for the α-^{40}Ca system. The experimental differential cross sections $d\sigma_i^{\rm exp}/d\Omega_d$ are available for about 30 levels in the excitation energy region considered. The $l_{\alpha,i}$ value (or equivalently the spin-parity) of the transition to a level i is then obtained by fitting $d\sigma_{n_\alpha l_\alpha}/d\Omega_d$ to $d\sigma_i^{\rm exp}/d\Omega_d$. The spectroscopic factors S_i are then determined as

$$S_i=\frac{d\sigma_i^{\rm exp}}{d\Omega_d}\Big/\frac{d\sigma_{n_\alpha l_\alpha}}{d\Omega_d}\ . \tag{20}$$

Figures 2 and 3 show the results of the fit of the calculated $d\sigma_{n_\alpha l_\alpha}/d\Omega_d$ to $d\sigma_i^{\rm exp}/d\Omega_d$ for $E_{\rm lab}=28$ and 50 MeV, respectively. As noted in Sec. III B, the calculated $d\sigma_{n_\alpha l_\alpha}/d\Omega_d$ is rather sensitive to the lower cutoff radius R_c, particularly for the 50 MeV case. We demonstrate this in Fig. 4, where plotted are $d\sigma_{n_\alpha l_\alpha}/d\Omega_d$ for $(n_\alpha,l_\alpha)=(6,0)$ and (5,2) with varied R_α values. As seen, $d\sigma_{n_\alpha l_\alpha}/d\Omega_d$ changes quite sensitively as R_c is changed. The R_c values were then fixed in such a way that $d\sigma_{n_\alpha l_\alpha}/d\Omega_d$ fits the experimental data for known J^π states as far as possible. The R_c values determined this way for $E_{\rm lab}=50$ MeV have already been given in Fig. 1. For $E_{\rm lab}=28$ MeV, the results are not sensitive to the R_c value, and therefore we simply set $R_c=0$ in this case.

The resultant J^π and S values are summarized in Table II. Note that the S_i values for 50 MeV are not the original values deduced directly from the experimental cross section by using Eq. (20), but are divided by 1.5. This division was made, since the values deduced directly from the 50 MeV experimental data are systematically larger by about 1.5 than those obtained from the 28 MeV data and also many of the values including that of the ground state are otherwise larger than unity. Table II includes also information on the spin-parity obtained from the (α,γ) [19] and the ^{46}Ti(p,t)^{44}Ti reaction [20]. J^π values that are unable to be fixed with certainty are given in parentheses. It should be noted at this stage that the higher the incident energies, the less characteristic the calculated angular distributions are for different l_α, making the determination of the l_α value more difficult.

With the modification discussed above, the S_i factors determined from the present analyses of the $E_{\rm lab}=28$ and 50 MeV data agree fairly well with each other, and also those determined previously in Ref. [3] for the 28 MeV

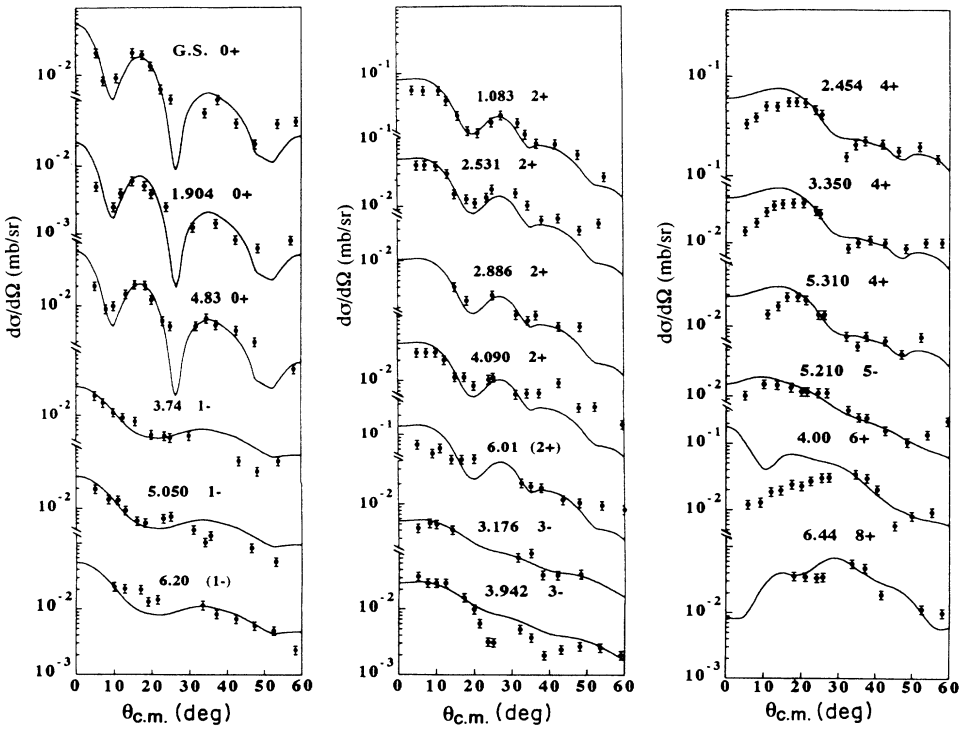

FIG. 2. Calculated angular distributions in comparison with the experimental data for $E_{\rm lab}=28$ MeV.

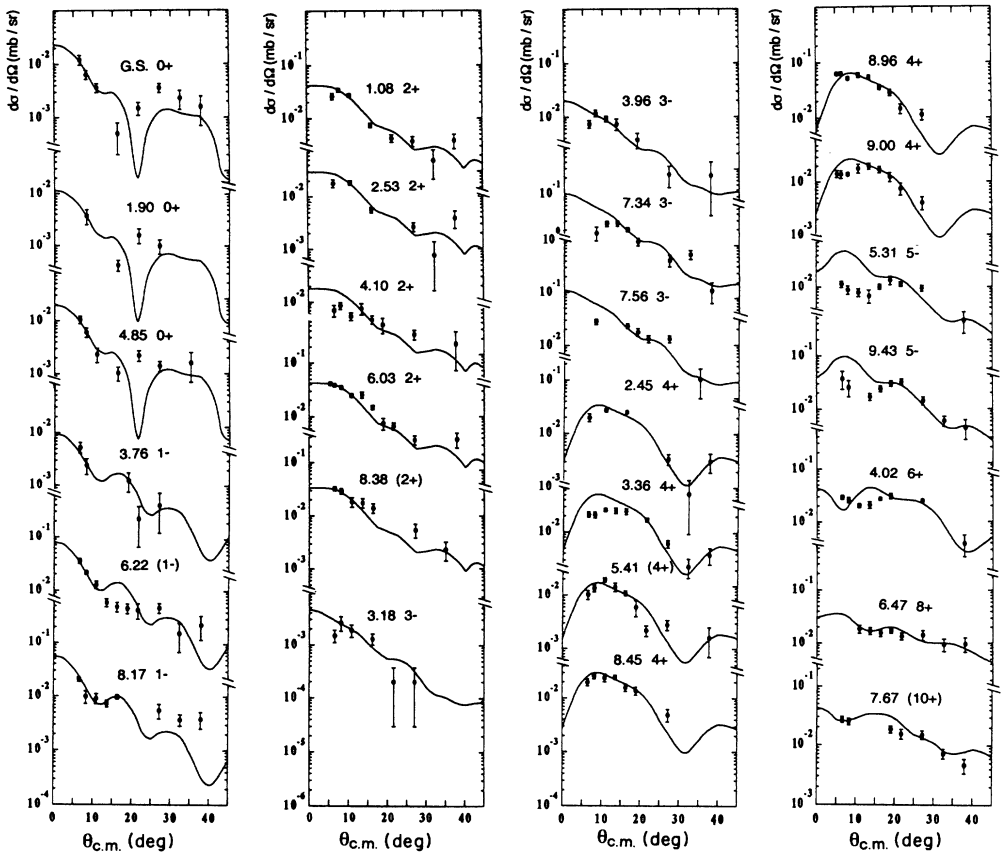

FIG. 3. Calculated angular distributions in comparison with the experimental data for $E_{lab}=50$ MeV.

data. Note, however, that the S_i factors obtained in Ref. [4] (from the 50 MeV data) are smaller by an order of magnitude as compared with those obtained in the present work. The reason for this can be ascribed to the distorting potentials used. As already noted before, the potentials used in Ref. [4] are largely different from the elastic potentials; the radius parameters of the real potentials for the ^{6}Li and d channels were modified from their elastic values of 1.30 and 1.05 fm to 1.05 and 1.35 fm, respectively. We have confirmed that such modifications result in a dramatic increase of contributions from the lower partial waves to the cross section, making the magnitude of the calculated unit single particle cross sections very large, and hence the S_i factors small.

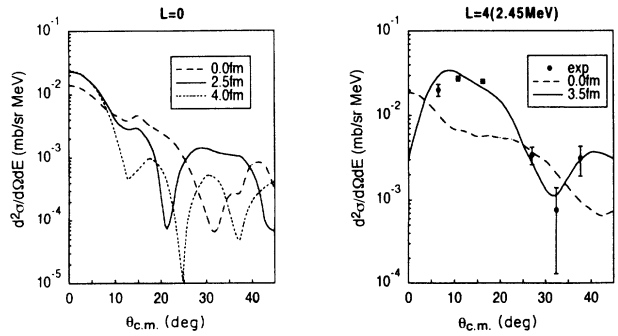

FIG. 4. Calculated angular distributions with and without cutoff in the integration over the radial coordinate in the α channel. The results show the sensitivity on the lower cutoff.

It may be worthwhile to give a comment here that at 28 MeV the reaction is a good angular momentum matched reaction; however, at 50 MeV it becomes a highly mismatched one. In fact, the difference between the grazing partial waves in the incident and outgoing channels is about 4 at 28 MeV, while the difference becomes 12 at 50 MeV. Therefore, at 28 MeV the reaction is still a good surface reaction, and this explains why the calculated cross section is rather insensitive to the lower cutoff as already remarked above. This is not the case for 50 MeV, however, and because of this the incident partial waves that are much lower than the grazing partial wave contribute importantly to the cross section. The normalization factor 1.5 needed to be introduced for the 50 MeV case may be ascribed to this undesirable feature of the reaction at 50 MeV.

IV. CLUSTER STRUCTURE IN ^{44}Ti

A. S_i factors for $J^{\pi}=0^{+}$, 2^{+}, and 4^{+} states

We have obtained fairly reliable values of the S_i factors for a number of states, particularly 0^{+}, 2^{+}, and 4^{+} states. Table III summarizes the values. We listed there the values only for those states whose spin-parity is certain. One remarkable feature of these S_i factors is that the summed strength reaches approximately 2 for all the

TABLE II. J_i^π and S_i values obtained from the present analysis, together with spin-parities assigned from the (α,γ) and the ^{46}Ti$(p,t)^{44}$Ti reaction. J_i^π values whose assignments are not certain are given in parentheses.

	^{40}Ca(α,γ) Ref. [19]	^{46}Ti(p,t) Ref. [20]	^{40}Ca(^{6}Li,d) Ref. [4]	^{40}Ca(^{6}Li,d)^{44}Ti Present work			
				$E=50$ MeV		$E=28$ MeV	
E_{ex}	J^π	J^π	J^π	J^π	S_α	J^π	S_α
g.s.	0^+	0^+	0^+	0^+	0.99	0^+	0.94
1.08	2^+	2^+	2^+	2^+	0.70	2^+	0.48
1.90	0^+	0^+	0^+	0^+	0.33	0^+	0.32
2.45	4^+	4^+	4^+	4^+	0.43	4^+	0.50
2.53	2^+	$(2^+$	2^+	2^+	0.47	2^+	0.32
3.18	(3^-)	(2^+)	3^-	3^-	0.03	3^-	0.01
3.37	4^+	4^+	4^+	4^+	0.51	4^+	0.50
3.76	(2^+)		1^-	1^-	0.11	1^-	0.14
3.96	3^-	3^-	3^-	3^-	0.15	3^-	0.04
4.02	6^+	$(5^-,6^+)$	6^+	6^+	0.58	6^+	0.56
4.10			2^+	2^+	0.31	2^+	0.21
4.85			0^+	0^+	0.75	0^+	1.00
5.21						5^-	0.01
5.31			5^-	(5^-)	0.14	(4^+)	0.30
5.41		(2^+)	3^-	(4^+)	0.17		
6.03		(4^+)	2^+	2^+	0.83	2^+	0.80
6.22			1^-	(1^-)	1.02	(1^-)	0.25
6.47	(8^+)		8^+	8^+	0.33	8^+	0.56
7.34			3^-	3^-	0.51		
7.56			(3^-)	3^-	0.73		
7.67	(10^+)	(4^+)	$6^+(N=14)$	10^+	0.43		
8.04	(12^+)		$8^+(N=14)$	(12^+)	2.43		
8.17			1^-	(1^-)	0.73		
8.38			2^+	(2^+)	0.56		
8.45			3^-	4^+	0.30		
8.54			$6^+(N=14)$				
8.96			2^+	4^+	0.38		
9.00			4^+	4^+	0.31		
9.19			6^+				
9.43			5^-	5^-	0.30		

three spin states, greatly exceeding the sum rule limit of the $N=12$ strength. If one takes this result seriously, we are forced to conclude that there is considerable mixing of the $N=14$ strength even in such low-lying states as considered in Table III.

Take, as an example, the 0^+ state. The S value of the ground state (0.97 in the average) is very close to unity, implying that the state already exhausts the $N=12$ strength. The next 0^+ state with a large S_i factor is found at $E_{ex}=4.85$ MeV. The average S value of this state is 0.88. This value may then be ascribed to that of $N=14$, which means that the main component of the 4.85 MeV state is the 0^+ state of the $N=14$ band. If one assumes that this is indeed the case, the resultant fit of the calculated angular distribution to experiment is improved. This is seen in Fig. 5, where are shown the theoretical cross sections obtained by repeating the calculation using $V_\alpha=212$ MeV instead of 182 MeV used before (see Table I). With this new V_α value, the predicted position of the 0^+ state of $N=14$ agrees with the experimental value of 4.85 MeV. The fit obtained in Fig. 5 is indeed better than that obtained in Figs. 2 and 3. The

TABLE III. A summary of S_i factors for relatively low-lying $J^\pi=0^+$, 2^+, and 4^+ states.

		S_α		
J^π	E_{ex} (MeV)	50 MeV	28 MeV	Ave.
0^+	g.s.	0.99	0.94	0.97
	1.90	0.33	0.32	0.33
	4.85	0.75	1.00	0.88
				2.17
2^+	1.08	0.70	0.48	0.59
	2.53	0.47	0.32	0.40
	4.10	0.31	0.21	0.26
	6.03	0.83	0.80	0.82
				2.06
4^+	2.45	0.43	0.50	0.47
	3.37	0.51	0.50	0.51
	8.45	0.30		0.30
	8.96	0.38		0.38
	9.00	0.31		0.31
				1.96

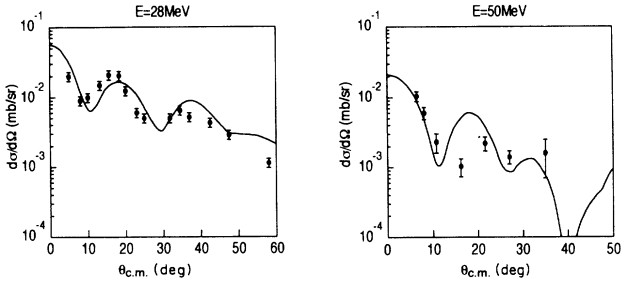

FIG. 5. The theoretical angular distributions for the 4.85 MeV 0^+ states obtained by assuming that the state is the $N=14$ state in comparison with the experimental data.

newly obtained averaged S_i value is 0.82 (0.66 and 1.07 for $E_{\rm lab}=28$ and 50 MeV, respectively). The values remain essentially the same as those obtained before with $N=12$. Similar observations may also be made for the 2^+ and 4^+ states: The α-transfer strength for the lowest two 2^+ and 4^+ states exhausts the total $N=12$ strength, while the rest of the higher excited states may carry the $N=14$ strength. We note that to assume a larger V_α value for the higher excited $N=14$ band as made above is not totally unreasonable. Rather it is consistent with the strong energy dependence coming from the threshold anomaly [21].

The results obtained in Table III indicate also that the strengths, particularly of the $l_\alpha=2$ and 4 transitions, are spread among a few to several states. Ohkubo [10] has suggested that the 0^+, 2^+, and 4^+ states at 1.91, 2.53, and 3.37 MeV may be the members of the $N=12$ cluster states built on the first excited 0^+ state of ^{40}Ca at 3.35 MeV. The latter 0^+ excited state can be considered as a four-particle–four-hole (4p-4h) state, i.e., the $N=12$ cluster state built upon the ground state of ^{36}Ar. This implies that the above-mentioned states in ^{44}Ti are 8p-4h states. If these states are pure, the S_i factors, of course, vanish. As seen in Table III, this is not the case; these states have significant S_i values, indicating that the 8p-4h states are fairly strongly mixed with those of the 4p states of $N=12$.

We note that the argument given above is based on our presumption that the absolute magnitudes of the S_i factors given in Tables II and III are reliable. The absolute magnitude of the S_i factors are, however, within a theoretical uncertainty of, say, a factor of 2, and therefore we cannot rule out the possibility that the strength observed in the excitation energy region considered may all come from the $N=12$ cluster states. If this is indeed the case, our conclusion is altered to the statement that the $N=12$ cluster strength for the 0^+, 2^+, and 4^+ states is extremely widely spread.

B. Positive parity states of the $N=12$ band

The idea has now been widely accepted that the 0^+–12^+ states observed at $E_{\rm ex}=0.0$, 1.08, 2.45, 4.02, 6.47, 7.67, and 8.04 MeV are the α-cluster states of $N=12$ [4,6,7]. The results of the present analysis support the idea with, however, a few exceptions: The first is that these states cannot be considered to be pure $N=12$ states, but are mixed considerably with other states, for instance, with the 8p-4h states as already discussed in Sec. IV A. The second point is that the S_i value (2.4) obtained for the 8.04 MeV 12^+ state is unreasonably large, and also that the fit of the calculated angular distribution to the data is extremely poor. Therefore, the state cannot be assigned to as a 12^+ state, although the (α,γ) [19] reaction data strongly indicate that a 12^+ state exists at that excitation energy. Perhaps the state might be a doublet.

Yamaya *et al.* [4] suggested that the 10^+ state at 7.67 MeV state might not be a 10^+, but rather a 6^+ state of the $N=14$ band. The suggestion came from their difficulty in reproducing the measured angular distribution of this state with $l_\alpha=10$. We had, however, no difficulty of reproducing it with $l_\alpha=10$. The resultant S_i factor of 0.43 seems to be reasonable in view of the spreading seen in the lower spin states. It is likely that the S_i factors of the $N=12$ band spread more as the J_i value increases, the tendency predicted theoretically by Arima [8] and others [22].

C. Negative parity states

The question as to where the $N=13$ band is located has been one of the crucial issues of the α-cluster structure in ^{44}Ti. Yamaya *et al.* [4] have identified the 1^-, 3^-, and 5^- members of this band at 6.22, 7.34, and 9.43 MeV, respectively. The results of the present analysis more or less confirm this. It should be noted, however, that the fit to the 6.22 MeV 1^- state is not so good as that obtained for other spin states. Further, the S_i factors obtained from the 28 and 50 MeV data differ considerably, and therefore it is difficult to assign the spin-parity of this state definitely. We also note that the S_i factors 0.52 and 0.3 of the 3^- and 5^- states, respectively, are only a fraction of the total strength, indicating that the strength is considerably spread into other states. In fact, we have identified several 3^- states with considerable S_i values. The spreading is also seen in the 1^- state; there is another state with a non-negligible S_i value observed at 3.76 MeV.

The 1^- and 3^- states observed at 3.76 and 3.96 MeV, respectively, may be interpreted as $N=12$ cluster states built on the 3^- core excited state. The nonzero S_i factors obtained for these states may suggest that these states mix with the states of $N=13$.

V. SUMMARY

Analyses have been made of ^{40}Ca(^{6}Li,d)^{44}Ti reaction data at incident energies of 28 and 50 MeV [3,4] within the framework of the breakup-fusion approach. The approach allows us to define the unit single particle cross sections in both bound and unbound regions on a single footing. Such unit single particle cross sections were calculated by using distorting potentials that are consistent with the elastic scattering data (elastic potentials), and then applied to analyze the experimental cross sections. During the course of the study, we have observed that the calculated angular distributions, particularly those at higher incident energies, are sensitive to the lower cutoff

of the radial integration in the α channel. With an appropriate choice of the lower cutoff parameter, we have been able to reproduce the observed angular distributions with the elastic potentials. From the analyses of the data, $l_{\alpha,i}$ values and spectroscopic factors S_i have been extracted for the individual final states up to $E_{ex} \approx 10$ MeV.

The S_i values obtained from the 28 and 50 MeV data and also those determined in Ref. [3] agreed fairly well with each other, but differed largely from those determined in Ref. [4]. The latter difference is then shown to be ascribed to the use of the distorting potentials in Ref. [4] that are quite different from the elastic potentials.

The most striking feature of the resultant S_i factors for the 0^+, 2^+, and 4^+ states is that with a reasonable assumption that the ground 0^+ state has an S factor close to unity, the sum over the S_i factors for the low-lying states below the excitation energies of 4.85, 6.03, and 9.00 MeV for the 0^+, 2^+, and 4^+ states, respectively, becomes approximately 2, suggesting that these states exhaust not only the total strength of the $N=12$ band, but also that of the $N=14$ band. This further implies that the $N=14$ states appear at a much lower excitation energy region than that predicted from the "unique potential" of Ref. [14]. Another remarkable feature is that such single 4p-type α-cluster states of $N=12$ and 14 are fairly strongly mixed with cluster states of the 8p-4h character.

At this stage, however, we may not exclude completely the possibility that the absolute spectroscopic factors deduced in the present analysis have a theoretical uncertainty of a factor of 2, and that the α-transfer strength observed in the excitation energy region considered all originates from the $N=12$ cluster states. Further studies are needed in order to obtain a more concrete conclusion on this question.

As the incident energy increases, the angular distributions become less sensitive to the transferred orbital angular momentum l_α. This has made it more difficult to assign the l_α value and hence the spin-parity of the final states unambiguously. In this regard, it would be helpful if more elaborate data, e.g., those of γ rays taken in coincidence with the outgoing deuteron, were to be taken.

In the present study, we have confined our calculation to the reaction leading to a rather low excitation energy region of the final nucleus ^{44}Ti. It would, however, be quite interesting to extend it further into the continuum. There it is expected that the α-cluster picture of the $^6\text{Li} \rightarrow \alpha + d$ process becomes more valid, and therefore we may make a more critical test of the absolute magnitude of our calculated cross section against the experimental data. Unfortunately, the data for such a test are not available at present. It is hoped that such data will soon become available.

We would like to express our sincere thanks to Dr. Yamaya for his interest in this work and also for sending numerical values of the 50 MeV data. We wish also to thank Dr. Luisa Zetta and Dr. Paolo Guazzoni for our use of their data prior to the publication. We are also thankful to Professor W. R. Coker for his careful reading of the manuscript and valuable comments. This work was supported in part by the U.S. Department of Energy under Contract No. DE-FG05-84-ER40145.

[1] T. Udagawa, Y. J. Lee, and T. Tamura, Phys. Lett. B **196**, 291 (1987).
[2] T. Udagawa, Y. J. Lee, and T. Tamura, Phys. Rev. C **39**, 1 (1989).
[3] H. W. Fulbright, C. L. Bennet, R. A. Lindgren, R. G. Markham, S. C. McGuire, G. C. Morrison, U. Strohbusch, and J. Töke, Nucl. Phys. **A284**, 329 (1977).
[4] T. Yamaya, S. Oh-ami, M. Fujiwara, T. Itahashi, K. Katori, M. Tosaki, S. Saito, S. Hatori, and S. Ohkubo, Phys. Rev. C **42**, 1935 (1990).
[5] F. Michel, G. Reidemeister, and S. Ohkubo, Phys. Rev. Lett. **57**, 1215 (1986).
[6] F. Michel, G. Reidemeister, and S. Ohkubo, Phys. Rev. C **38**, 2377 (1988).
[7] A. C. Merchant, K. F. Pál, and P. E. Hodgson, J. Phys. G **15**, 605 (1989).
[8] A. Arima, in *Proceedings of the Topical Conference on Physics of Medium Light Nuclei,* edited by P. Blasi and R. Ricci (Editrice Compositori, Bologna, 1979), p. 19.
[9] T. Wada and H. Horiuchi, Phys. Rev. C **38**, 2063 (1988).
[10] S. Ohkubo, in *Proceedings of 6th International Conference on Nuclear Reaction Mechanisms,* edited by E. Gadioli (Universita Degli Studio Di Milano, 1991), p. 396.
[11] Th. Delbar *et al.*, Phys. Rev. C **18**, 1237 (1978).
[12] See, for instance, G. G. Satchler, *Direct Nuclear Reactions* (Oxford University Press, Oxford, 1983).
[13] L. T. Chua, F. D. Becchetti, J. Jänecke, and F. L. Milder, Nucl. Phys. **A237**, 243 (1976).
[14] W. W. Daehnick, J. D. Childs, and Z. Vrcelj, Phys. Rev. C **18**, 1237 (1978).
[15] R. Ent *et al.*, Phys. Rev. Lett. **57**, 2367 (1986).
[16] K. Varga and R. G. Lovas, Phys. Rev. C **43**, 1201 (1991).
[17] G. F. Perry and A. M. Saruis, Nucl. Phys. **A70**, 225 (1970).
[18] D. Brink and J. J. Castro, Nucl. Phys. **A216**, 109 (1973).
[19] W. R. Dixon, R. S. Storey, and J. J. Simpson, Nucl. Phys. **A202**, 579 (1973); J. J. Simpson, W. R. Dixon, and R. S. Storey, Phys. Rev. Lett. **31**, 946 (1973); W. R. Dixon, R. S. Storey, and J. J. Simpson, Phys. Rev. C **15**, 1896 (1977).
[20] J. Rapaport, J. B. Ball, R. L. Auble, T. A. Belote, and W. E. Dorenbusch, Phys. Rev. C **5**, 453 (1972).
[21] C. Mahaux, H. Ngo, and G. R. Satchler, Nucl. Phys. **A456**, 134 (1986).
[22] T. Yamada, Phys. Rev. C **42**, 1432 (1990).